11th International Symposium on Turbulence and Shear Flow Phenomena (TSFP11)
Southampton, UK, July 30 to August 2, 2019

SURFACE TOPOLOGY EFFECTS ON THE TRANSVERSE GALLOPING BEHAVIOR OF RECTANGULAR CYLINDERS

Mark A. Feero, Ahmed M. Naguib & Manoochehr M. Koochesfahani
Department of Mechanical Engineering
Michigan State University
East Lansing, MI, 48823
feeromar@egr.msu.edu

ABSTRACT

The effect of geometry on the transverse galloping behavior of rectangular cylinders was studied experimentally for Reynolds numbers between 1,000 and 10,000. In particular, a comparison was made between a rectangular cylinder with rounded corners and a smooth surface, and the same baseline geometry with added surface topology synthesized from two-dimensional Fourier-modes. The effect of the amplitude of the topological surface height was investigated. From measurements of the normal (galloping direction) force coefficient variation with angle-of-attack, it was found that the added surface topology generally had a destabilizing effect relative to the smooth cylinder. At the lowest Reynolds number, the smooth cylinder was stable, while the cylinders with added topology were unstable with respect to galloping. For Reynolds numbers from 5,000 to 10,000, the added topology did not cause a similar instability. However, there was a monotonic increase in the slope of the normal force coefficient at zero angle-of-attack with increasing surface height amplitude, thus moving the geometry closer to the instability threshold. This effect diminished as Reynolds number increased. Overall, for the range of parameters investigated herein, the cylinder with larger topology amplitude exhibited more favorable galloping resistance characteristics than the one with smaller topology.

INTRODUCTION

An elastically mounted cylinder with non-circular cross section may be susceptible to a flow-induced oscillation known as galloping. This is a result of the fact that the aerodynamic forces acting on the body vary with its orientation to the oncoming flow. This is described schematically in Figure 1 for a rectangular cylinder elastically mounted in the transverse direction (y-direction). The lift and the drag forces, F_L and F_D, respectively, will be oscillatory in time due to the oscillation of the body at a velocity $\dot{y}$. The normal force coefficient in the y-direction is related to the lift and the drag coefficients, *viz*:

$$C_y = \frac{F_y}{1/2\rho U_\infty^2 dl} = -\frac{1}{\cos^2\alpha}(C_L\cos\alpha + C_D\sin\alpha), \quad (1)$$

where $C_L = F_L/(1/2\rho U_{\text{rel}}^2 dl)$ and $C_D = F_D/(1/2\rho U_{\text{rel}}^2 dl)$ are the lift and the drag coefficients, respectively, α is angle-of-attack, U_∞ is the steady freestream velocity, U_{rel} is the instantaneous oncoming velocity relative to the cylinder, ρ is the density, d is the cylinder width and l is the cylinder span. If the oscillation is such that C_y increases with α, this produces negative fluid damping and the structure may become unstable. Mathematically, the necessary aerodynamic condition for transverse galloping is $\partial C_y/\partial\alpha > 0$. This phenomenon can affect structures such as ice coated power lines, bridge decks and stalled wings (Blevins, 2001). Another type of structure that may be susceptible to galloping is the parachute suspension line used in precision airdrop systems. A typical suspension line has a non-circular cross section that resembles a rectangle with side ratio $c/d = 2$ – 3 (where c is chord length) and rounded corners (Siefers *et al.*, 2013). The unsteady forces arising from potential galloping of the suspension lines could contribute substantially to the overall aerodynamic performance of the airdrop system, since the lines have been shown to significantly affect the total drag (Bergeron *et al.*, 2009). Understanding the galloping behavior of such a geometry is therefore fundamental to the prediction and mitigation of this aero-elastic instability.

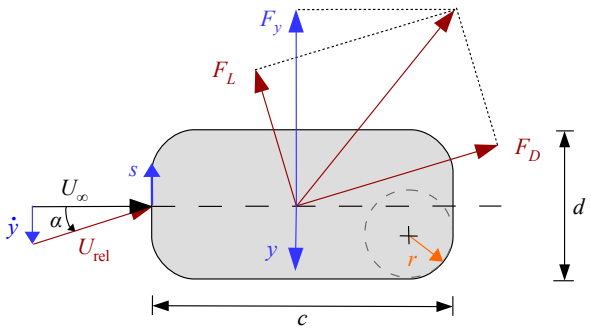

Figure 1: Rectangular cylinder cross-section geometry and forces acting on the body when oscillating at a velocity $\dot{y}$ in the transverse direction.

The goal of the present work is to investigate the galloping behavior of rectangular cylinders that approximate the geometry of parachute suspension line. While work has been done in the past on the galloping behavior of rectangular cylinders (e.g., Mannini *et al.*, 2014; Washizu *et al.*, 1978; Parkinson & Brooks, 1961), these experiments

are generally performed at Reynolds numbers in the range $Re_d > 2\times10^4$, where $Re_d = U_\infty d/\nu$ and ν is kinematic viscosity. The relevant Reynolds number range for parachute lines is 1,000 to 10,000 and is the focus of this study. Majority of the previous studies regarding the galloping behavior of rectangular cylinders considered only those with smooth surfaces. However, a parachute line is often formed by braiding smaller lines, therefore the surface is not smooth but has variations in height. An investigation regarding this type of geometry has not previously been performed, except by Siefers *et al.* (2013) and Siefers *et al.* (2014) who analyzed only the vortex shedding frequencies and flow visualization of parachute suspension line. This study investigates the aerodynamic forces and galloping behavior of rectangular cylinders with smooth surfaces and those with an idealized surface topology with parameters approximating that of a parachute line. Since the time scale of galloping oscillations is often substantially higher than those of the dominant flow features (e.g., vortex shedding) (Blevins, 2001), the classical assumption of quasi-steady behavior allows the results from static wind-tunnel tests to be used to describe the variation of aerodynamic forces with α. Thus, measurements of aerodynamic loads are performed on rigidly mounted, static models with varying angle-of-attack.

EXPERIMENTAL SETUP

Experiments are conducted in a low-speed, low-turbulence open return wind tunnel located in the Flow Physics and Control Lab at Michigan State University. After passing through a section of flow management devices and a 10:1 contraction, the flow enters a 355 mm by 355 mm square test section that is 3 m long. The experiments in this work span a Reynolds number range of $Re_d = 1{,}100$ to $10{,}000$, which corresponds to $U_\infty \approx 0.8$ m/s to 7.5 m/s. Over this range of freestream velocities, the mean turbulence intensity in the test section is 0.1% for a frequency range above 0.5 Hz. The mean freestream velocity is measured upstream of the model using a pitot-static tube.

The geometric parameters of the models under investigation are selected to approximate typical flat parachute suspension line both with and without the surface topology representative of braided cables. Based on the work of Siefers *et al.* (2013), the basic cross-sectional dimensions of the models used in this study are $c/d = 2.5$ and $r/d = 0.5$. The surface topology of the braided cables is approximated using two-dimensional Fourier-modes to describe the height of the surface relative to the local nominal smooth cylinder. The local surface height, ε, is defined as:

$$\frac{\varepsilon}{\varepsilon_o} = \frac{1}{2}\cos\left[2\pi\left(\frac{s}{\lambda_s}+\frac{z}{\lambda_z}\right)\right] + \frac{1}{2}\cos\left[2\pi\left(\frac{s}{\lambda_s}-\frac{z}{\lambda_z}\right)\right], \tag{2}$$

where s and z are the wall-tangential and axial coordinates, respectively, ε_o is the surface height amplitude, and λ_s and λ_z are the wavelengths in the s and z directions, respectively. The s-direction wavelength can also be defined as $\lambda_s = P/n$, where n is the number of wavelengths in the s-direction and P is the perimeter. In order to avoid discontinuities in the surface, n is selected as an integer. This approach gives a rigorous definition of the surface topology and allows systematic modification of specific topological parameters to investigate their effects, as opposed to a heuristic method of approximating a braided cable topology. To create a model with added topology, the height variation with s and z is superimposed on a nominal cross-sectional shape, such as the one shown in Figure 1. The baseline model with topology (Figure 2) has $\varepsilon_o/d = 5\%$, $n = 10$ ($\lambda_s/d = 0.61$) and $\lambda_z/\lambda_s = 1.5$, and approximates the geometry of 600 lb load-capacity *Dacron* cable. The effect of surface height amplitude is investigated using a second model with a higher amplitude of $\varepsilon_o/d = 10\%$ and the same n and λ_z. A smooth model with no topology ($\varepsilon_o/d = 0$) is machined from aluminum, while the models with topology consist of a 3D printed plastic outer sleeve around a solid aluminum spar. The solid aluminum spar corrects any warping or twisting in the 3D printed parts and maintains spanwise straightness over time.

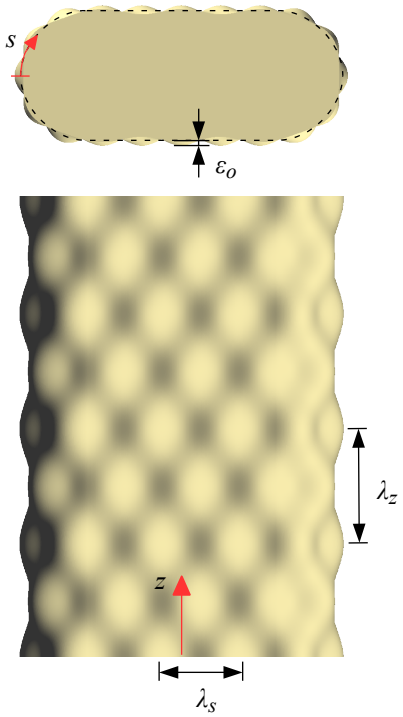

Figure 2: Top and cross-sectional views of the cylinder with $\varepsilon_o/d = 5\%$, $n = 10$ and $\lambda_z/\lambda_s = 1.5$. The dashed line indicates the nominal smooth cylinder.

The models have dimensions $d = 20$ mm and $l = 320$ mm, which spans the height of the test section between circular end plates. The end plates are fixed to the tunnel walls and have a diameter of $15d$ and a 30° chamfered edge. In addition to the large end plates, small end plates with $4.5d$ diameter and 0.75 mm thickness were fixed to the ends of the model. These small end plates were necessary to eliminate axial flow effects due to air being drawn into the test section from the surroundings through the 20 mm × 30 mm holes in the end plates. The hole in the upper end plates allows the model connection shaft to pass through the end plate and move freely. The nominal solid blockage of the models at $\alpha = 0°$ is 5%.

Mean lift and drag forces on the models were measured using a custom designed one-component force balance (Feero *et al.*, 2019). This force balance was designed to allow accurate load measurement despite the low Reynolds number range where commercially available load

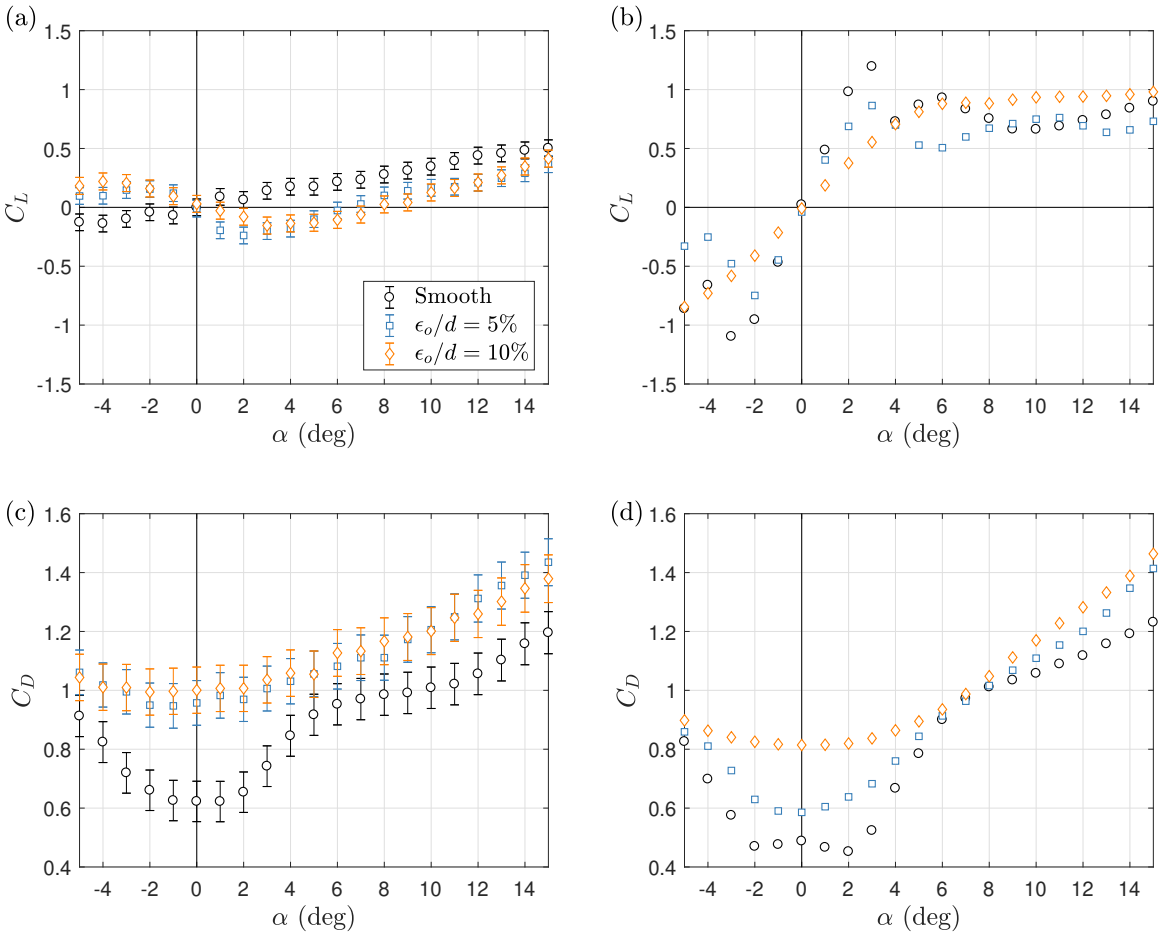

Figure 3: Lift and drag coefficient variation with angle-of-attack for the smooth and topology models. (a) & (c): $Re_d = 1{,}100$. (b) & (d): $Re_d = 10{,}000$. For $Re_d = 10{,}000$, error bars are less than the marker size.

cells would be inadequate. To give a sense of scale, a drag coefficient $C_D = 1$ for the models used in this study corresponds to a drag force ranging from approximately 2.5 to 200 mN over $Re_d = 1{,}100$ to 10,000. The force balance is comprised of a four bar parallelogram linkage from which the model is vertically suspended. A horizontal aerodynamic force on the model causes the linkage/model to displace primarily in the horizontal direction, and this displacement is measured by a non-contact laser displacement sensor. Given the stiffness of the force balance, which depends on model weight, it provides a resolution of 0.19 mN. For C_D or C_L of 1, the typical accuracy of the force measurements ranges from 0.2 mN to 2.3 mN over $Re_d = 1{,}100$ to 10,000. The entire force balance can be rotated to switch between lift and drag measurement. Forces were measured for a range of α, where the model angle was varied using a step-servo motor with a resolution of 0.02°.

RESULTS

The lift and drag forces were measured for $-5° \leq \alpha \leq 15°$ at $Re_d = 1{,}100$, 2,500, 5,000, 7,500 and 10,000 for each of the models. Results at $Re_d = 1{,}100$ and $Re_d = 10{,}000$ are shown in Figure 3. For the smooth model at $Re_d = 10{,}000$, C_L varies with α in a way that is similar to a streamlined body; that is, C_L increases as α increases from 0° up to a maximum at 3° and then experiences a moderate decrease. A second peak occurs in C_L at $\alpha = 6°$, which is followed by C_L increasing slightly with α. The $\epsilon_o/d = 5\%$ model displays a similar trend, although the maximum C_L is reduced relative to the smooth case. This case also exhibits some asymmetry between positive and negative angles of attack, the reason for which is unknown. As the surface height amplitude increases to $\epsilon_o/d = 10\%$, no peaks in C_L are observed but rather the slope of C_L smoothly decreases and the curve approximately plateaus at 6°. For small values of α, below that of the first peak and the plateau, the slope of the lift curve decreases with increasing topology amplitude.

A considerable change in the overall behavior in C_L is observed for all geometries when Re_d is reduced to 1,100. At this Reynolds number, the slope in C_L near $\alpha = 0°$ is negative for all but the smooth case. The peak C_L magnitude is decreased substantially to approximately 0.2, whereas values up to 1.2 occur at $Re_d = 10{,}000$. Unlike the topology models, the smooth model experiences a nearly linear increase with α over the entire range.

The drag coefficient at $Re_d = 1{,}100$ and 10,000 is shown in Figure 3c and d, respectively. Examining first the smooth geometry at $Re_d = 10{,}000$, C_D is found to decrease slightly as α increases from 0° to 2°, beyond which it increases monotonically with α. Over $0° \leq \alpha \leq 15°$, C_D increases by more than a factor of two from approximately 0.5 to 1.2. When the $\epsilon_o/d = 5\%$ surface topology is added, the slope of C_D becomes exclusively positive over the entire

α range, and there is a small increase in C_D relative to the smooth case at $\alpha = 0°$. As ε_o/d increases from 5% to 10%, the C_D curve near $\alpha = 0°$ becomes substantially flatter and C_D at $\alpha = 0°$ increases from 0.6 to 0.8. Unlike C_L, when Re_d decreases to 1,100 there is not a reversal in the qualitative behavior of C_D. All the geometries maintain a slope in C_D that is approximately zero or positive over the α range. The $\varepsilon_o/d = 5\%$ and $\varepsilon_o/d = 10\%$ C_D curves are equivalent within the uncertainty and are flatter than the smooth case near $\alpha = 0°$.

The normal force coefficient, C_y, is computed from C_D and C_L according to equation 1. The variation in C_y with α for the entire Reynolds number range is shown in Figure 4 for each geometry. The solid lines in these plot are curve fits computed using either a cubic spline or a sliding cubic fit to smooth scatter in the data, where the latter case is typically used for $Re_d < 5{,}000$. Comparing the results at $Re_d = 1{,}100$ and 10,000 to Figure 3, it can be observed that C_y follows a tend quite similar to $-C_L$. Examining first the results for the smooth geometry in Figure 4a, the slope in C_y is negative at small angles-of-attack for all Re_d. This slope becomes increasingly negative as Re_d increases from 1,100 to 5,000, after which it begins to decrease is magnitude while remaining negative. Recall from the introduction that a body is unstable with respect to galloping when $\partial C_y \partial \alpha$ is positive. As Re_d increases above 1,100, a minimum in C_y begins to emerge near $\alpha \approx 3°$, with the value of this minimum reaching peak magnitude at $Re_d = 5{,}000$ – 7,500 before decreasing at $Re_d = 10{,}000$. The double peak behavior that was observed in C_L for $Re_d = 10{,}000$ remains present in C_y as double minima at approximately 3° and 6°. For $Re_d \geq 5{,}000$, C_y shows very little variation with Re_d at angles-of-attack above approximately 10°.

Figure 4b shows the C_y results for the $\varepsilon_o/d = 5\%$ geometry. The addition of this surface topology leads to an initially positive slope in C_y at $Re_d = 1{,}100$, and therefore a geometry that is unstable in the transverse galloping mode. As α increases, C_y reaches a peak after which the slope becomes approximately constant and negative. A transition occurs between $Re_d = 1{,}100$ and 2,500, as $\partial C_y/\partial \alpha$ at $\alpha = 0°$ becomes negative, indicating stability. For $Re_d \geq 2{,}500$, the shape in C_y is similar to that of the smooth geometry, however the magnitude of the C_y minimum is reduced. The effect of Re_d on this minimum magnitude is less than what is seen for the smooth case. A double minima behavior in C_y, as was observed for the smooth case at $Re_d = 10{,}000$, occurs for the $\varepsilon_o/d = 5\%$ geometry for $Re_d \geq 7{,}500$, with the second minimum occurring at a larger α relative to smooth case.

The effect of the largest topology amplitude $\varepsilon_o/d = 10\%$ on C_y is shown in Figure 4c. For $Re_d \leq 2{,}500$, the shape of C_y is similar to that of $Re_d = 1{,}100$ for $\varepsilon_o/d = 5\%$, although the magnitude of the maximum is decreased and it occurs at a slightly larger α. However, for $Re_d \geq 5{,}000$, C_y is distinctly different from both the smooth and $\varepsilon_o/d = 5\%$ cases. At $Re_d = 5{,}000$, a minimum in C_y is still observed, but C_y is substantially flatter at angles-of-attack near the minimum. Increasing Re_d from 5,000 to 10,000 results in a disappearance of this minimum, and a transition to C_y that is constantly decreasing with increasing α. Unlike the other two geometries, $\varepsilon_o/d = 10\%$ shows a a noticeable Reynolds number effect on C_y at large angle-of-attack, where C_y increases monotonically with increasing Re_d.

Figure 5 shows the effect of ε_o/d on the galloping criterion evaluated at $\alpha = 0°$, $\partial C_y/\partial \alpha|_{\alpha=0}$, over the entire

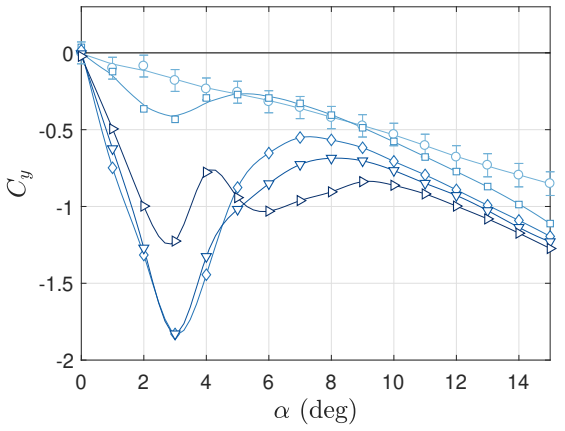

(a) Smooth

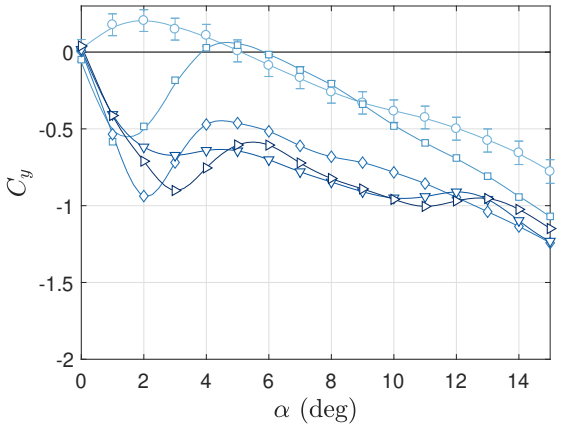

(b) $\varepsilon_o/d = 5\%$

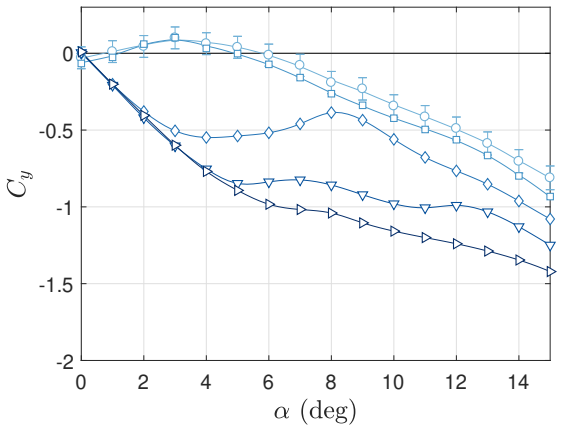

(c) $\varepsilon_o/d = 10\%$

Figure 4: Reynolds number effect on C_y versus α. Solid lines are curve fits to the data. Errorbars are less than the marker size for $Re_d \geq 2500$. (○) $Re_d = 1{,}100$, (□) 2,500, (◇) 5,000, (▽) 7,500, (▷) 10,000.

Reynolds number range. The derivative $\partial C_y/\partial \alpha$ is evaluated from the curve fits of $C_y(\alpha)$ described previously. The uncertainty in $\partial C_y/\partial \alpha$ is computed using a Monte Carlo method with 5×10^3 random samples. For the smooth cylinder, $\partial C_y/\partial \alpha|_{\alpha=0} < 0$ and thus this geometry is sta-

ble with respect to galloping over $1{,}100 \leq Re_d \leq 10{,}000$. As Re_d decreases from 10,000 to 5,000, $\partial C_y/\partial\alpha|_{\alpha=0}$ becomes increasingly negative, however a dramatic increase occurs when Re_d decreases to 2,500. Although the value of $\partial C_y/\partial\alpha|_{\alpha=0}$ remains negative, it becomes substantially closer to the instability threshold for $Re_d \leq 2{,}500$ compared with higher Reynolds number. The addition of the $\varepsilon_o/d = 5\%$ topology generally causes $\partial C_y/\partial\alpha|_{\alpha=0}$ to increase relative to the smooth case, indicating that this topology is generally destabilizing. This is particularly true at $Re_d = 1{,}100$, where $\partial C_y/\partial\alpha|_{\alpha=0} > 0$ and the geometry is unstable. For $Re_d \geq 5000$, $\partial C_y/\partial\alpha|_{\alpha=0}$ increases relative to the smooth case but does not become positive. Increasing ε_o/d to 10% generally has the same effect as $\varepsilon_o/d = 5\%$, except the larger amplitude makes the magnitude of $\partial C_y/\partial\alpha|_{\alpha=0}$ smaller. As a result, the increase in ε_o/d becomes destabilizing for $Re_d \geq 5{,}000$, since it causes the derivative to move closer to the instability threshold. On the other hand, for $Re_d = 1{,}100$, while the larger amplitude also makes the cylinder unstable, the decrease in the derivative magnitude makes the cylinder less prone to vibration since a larger critical reduced velocity would be require for the onset of oscillation. For all cases, the qualitatively different behavior between $Re_d = 1{,}100$ and $Re_d \geq 5{,}000$ is indicative of a transitional Re_d range that seems to encompass $Re_d = 2{,}500$. This may explain the lack of systematic trends for measurements at this Reynolds number. This includes the large change in $\partial C_y/\partial\alpha|_{\alpha=0}$ at $Re_d = 2{,}500$ and a behavior of the derivative with ε_o/d that is different from the low ($Re_d = 1{,}100$) and high ($Re_d \geq 5{,}000$) Reynolds number cases.

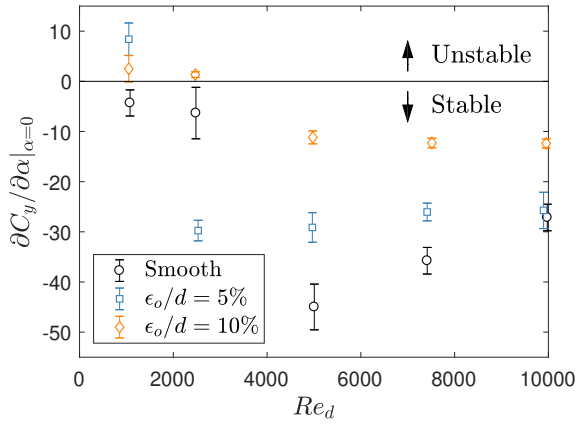

Figure 5: Effect of the surface height amplitude on the galloping criterion at $\alpha = 0^\circ$ with comparison to the smooth geometry.

The previous discussion regarding galloping stability was based on the value of $\partial C_y/\partial\alpha|_{\alpha=0}$, where $\partial C_y/\partial\alpha|_{\alpha=0} > 0$ indicates a body that would gallop from rest. In this case, a small disturbance causes the initial motion of the body and the oscillations of the body increase in time until non-linearities in the structure and/or fluid force drive the system towards a stable limit cycle of oscillations (Barrero-Gil *et al.*, 2009). However, for cases where $\partial C_y/\partial\alpha|_{\alpha=0} < 0$, the body may still be prone to galloping in a hard oscillation mode. This can occur if there are ranges of α away from 0° where $\partial C_y/\partial\alpha > 0$. Unlike "soft" oscillators, a hard oscillator requires a large initial disturbance to reach the basin of attraction of the limit cycle (Novak, 1972). The results in Figure 4 demonstrate for all three geometries, regions of $\partial C_y/\partial\alpha > 0$ exist for Reynolds numbers where $\partial C_y/\partial\alpha|_{\alpha=0} < 0$. The hard galloping behavior of each geometry is considered by examining $\partial C_y/\partial\alpha$ as a function of α, as shown in Figure 6. Results are shown at $Re_d = 5{,}000$ and 10,000, since each geometry is stable to galloping from rest over this Reynolds numbers range (Figure 5).

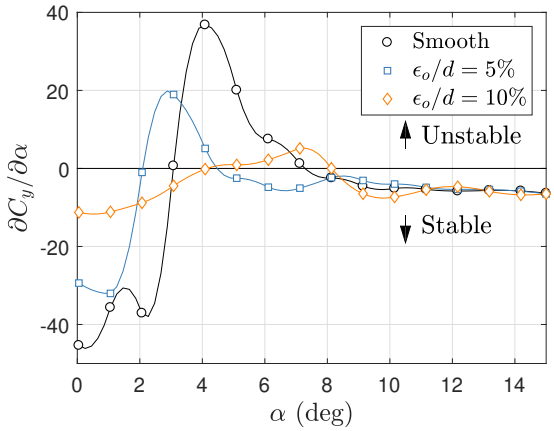

(a) $Re_d = 5000$

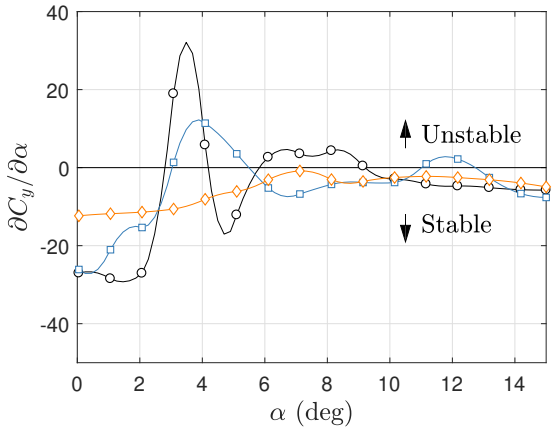

(b) $Re_d = 10{,}000$

Figure 6: Normal-force coefficient derivative variation with angle-of-attack for the smooth and the topology models.

At $Re_d = 5{,}000$, $\partial C_y/\partial\alpha$ for the smooth geometry is initially negative but becomes positive for α between approximately 3° and 7°. The angle where $\partial C_y/\partial\alpha$ first becomes positive (i.e., 3° for the smooth case) will be referred to as the galloping angle. The presence of the surface topology with $\varepsilon_o/d = 5\%$ results in a reduction in the galloping angle to approximately 2°. Therefore, the $\varepsilon_o/d = 5\%$ topology at $Re_d = 5{,}000$ makes the geometry more susceptible to hard galloping, as a smaller galloping angle corresponds to a smaller initial disturbance being capable to initiate oscillation. Increasing ε_o/d to 10% results in an increase in the

galloping angle relative to the smooth case, and also much smaller positive $\partial C_y/\partial\alpha$ magnitude. It is interesting to note that for $\alpha > 8^\circ$, surface topology has no effect on the slope of C_y as all three cases essentially collapse.

The effect of topology on $\partial C_y/\partial\alpha$ at $Re_d = 10,000$ is shown in Figure 6b. Unlike at $Re_d = 5,000$, the addition of surface topology does not make the body more susceptible to hard galloping relative to the smooth case. The $\varepsilon_o/d = 5\%$ topology has essentially the same galloping angle of $\sim 3^\circ$ as the smooth case. The large amplitude topology, $\varepsilon_o/d = 10\%$, at $Re_d = 10,000$ is an interesting case as it is completely stable over the investigated α range and is not susceptible to hard galloping. This is contrary to the destabilizing effect that increasing ε_o/d to 10% has on soft galloping. Although not shown for brevity, this was also the case for the $\varepsilon_o/d = 10\%$ geometry at $Re_d = 7,500$. A consistent trend over $5,000 \leq Re_d \leq 10,000$ is that the addition of surface topology leads to a decrease in the peak positive value of $\partial C_y/\partial\alpha$ relative to the smooth case (or the elimination of positive $\partial C_y/\partial\alpha$ altogether). For a given elastically mounted body, a decrease in the magnitude of positive $\partial C_y/\partial\alpha$ is associated with a decrease in the amplitude of oscillation and an increase in the critical reduced velocity required for galloping to occur (Blevins, 2001). The results at $Re_d = 10,000$ also show that unlike $Re_d = 5,000$, there are two ranges of α where the slope of C_y is positive for $\varepsilon_o/d < 10\%$. This is associated with the double peak behavior observed in Figure 4 for certain Re_d.

CONCLUSIONS

The effect of surface topology amplitude on the galloping instability of a rectangular cylinder with side ratio $c/d = 2.5$ and corner radius $r/d = 0.5$ was investigated experimentally for Reynolds numbers $Re_d = 1{,}100$ – 10,000. The topological parameter of interest was the surface height amplitude, ε_o/d; models were tested with two values of ε_o/d, 5% and 10%.

The smooth geometry showed a lift curve with positive slope near angle-of-attack $\alpha = 0^\circ$ over the entire Re_d range, while the added topology led to a shift from positive to negative slope with decreasing Re_d. The topology was found to increase drag at $\alpha = 0^\circ$ relative to the smooth case, with the increase being constant at $Re_d = 1{,}100$ and monotonically increasing with ε_o/d at $Re_d = 10,000$.

The smooth geometry was found to be stable over the investigated Reynolds number range, as indicated by $\partial C_y/\partial\alpha|_{\alpha=0} < 0$ (where C_y is the force coefficient in the galloping direction). In general, the results showed that the addition of surface topology had a destabilizing effect and caused an increase in $\partial C_y/\partial\alpha|_{\alpha=0}$. This increase lead to instability ($\partial C_y/\partial\alpha|_{\alpha=0} > 0$) for each topology geometry at $Re_d = 1{,}100$. In addition to the stability criterion for galloping from rest, $\partial C_y/\partial\alpha|_{\alpha=0}$, the hard galloping behavior was also investigated. With the exception of the $\varepsilon_o/d = 10\%$ geometry at high Reynolds number, all of the geometries showed susceptibility to hard galloping in cases where they were stable to galloping from a small disturbance. Increasing ε_o/d was found to decrease or eliminate the susceptibility to hard galloping. This feature along with a smaller magnitude of $\partial C_y/\partial\alpha|_{\alpha=0}$ renders the 10% more preferable to the 5% topology from the perspective of susceptibility to galloping, irrespective of the initiating disturbance level.

ACKNOWLEDGMENTS

The authors would like to acknowledge Mr. Kian Kalan who developed the code and methodology for generating 3D solid models of the cylinders with surface topology.

This project is funded through ARO grant number W911NF1710153. The views and conclusions contained in this document are those of the authors and should not be interpreted as representing the official policies, either expressed or implied, of ARO or the U.S. Government. The U.S. Government is authorized to reproduce and distribute reprints for Government purposes notwithstanding any copyright notation herein.

REFERENCES

Barrero-Gil, Antonio, Sanz-Andrés, A & Alonso, G 2009 Hysteresis in transverse galloping: the role of the inflection points. *Journal of Fluids and Structures* **25** (6), 1007–1020.

Bergeron, Keith, Ecklebe, Dan, McClure, Kyle, Johari, Hamid, Curlett, T & Pitman, B 2009 Parachute suspension line drag analysis. In *20th AIAA Aerodynamic Decelerator Systems Technology Conference and Seminar*.

Blevins, Robert D 2001 *Flow-induced vibration*, 2nd edn. Krieger Publishing Company.

Feero, Mark A, Naguib, Ahmed M & Koochesfahani, Manoochehr M 2019 Single-component force balance for the measurement of low-magnitude mean aerodynamic loads. Submitted.

Mannini, C, Marra, AM & Bartoli, G 2014 Viv–galloping instability of rectangular cylinders: Review and new experiments. *Journal of wind engineering and industrial aerodynamics* **132**, 109–124.

Novak, Milos 1972 Galloping oscillations of prismatic structures. *Journal of the Engineering Mechanics Division* **98** (1), 27–46.

Parkinson, GV & Brooks, NPH 1961 On the aeroelastic instability of bluff cylinders. *Journal of applied mechanics* **28** (2), 252–258.

Siefers, Timothy, Greene, Kara, McLaughlin, Thomas & Bergeron, Keith 2013 Wind and water tunnel measurements of parachute suspension line. In *51st AIAA Aerospace Sciences Meeting*.

Siefers, Timothy M, McLaughlin, Thomas E & Bergeron, Keith 2014 Wind tunnel characterization of fluid-structure interactions for various suspension lines. In *44th AIAA Fluid Dynamics Conference*.

Washizu, K, Ohya, A, Otsuki, Y & Fujii, K 1978 Aeroelastic instability of rectangular cylinders in a heaving mode. *Journal of Sound and Vibration* **59** (2), 195–210.